Journal of Mathematical Chemistry Vol. 38, No. 2, August 2005 (© 2005)
DOI: 10.1007/s10910-005-5409-5

The effect of a radical scavenger on the propagation of flames in an exothermic-endothermic system

Peter L. Simon* and Stephen K. Scott

Department of Chemistry
E-mail: simonp@cs.elte.hu

Serafim Kalliadasis

Department of Chemical Engineering

John H. Merkin

Department of Applied Mathematics, The University of Leeds, Leeds, LS2 9JT, UK

Received 17 March 2005; revised 31 March 2005

The propagation of a premixed laminar flame supported by an exothermic chemical reaction under adiabatic conditions but subject to inhibition through parallel endothermic chemical processes is considered. These consist of the endothermic decomposition of an inhibitor W leading to the formation of a 'radical scavenger' S, which acts as a catalyst for the removal of active radicals X through an additional termination step. The heat loss through the endothermic reaction and the action of the radical scavenger, represented by the parameters α and ρ, both have a strong quenching effect on wave propagation. The dependence of the flame velocity c on α and ρ is determined by numerical integration of the flame equations for a range of values of the other parameters. The (ρ, c) curve can have at least one turning point, the (α, c) curve can be monotone or it can have one or three turning points, depending on the values of the parameters β, representing the rate at which inhibitor is consumed, μ, the ratio of the activation energies of the reactants and the Lewis numbers. The additional feature caused by the scavenger is that the (α, c) curve has a turning point for any (μ, β) parameter pair if ρ is sufficiently large. A new feature of the model is that, for non-zero values of ρ, there can be four solutions below critical values of α. This behaviour is confirmed by a high activation energy analysis, which also reveals some additional features of the flame structure resulting from the presence of the radical scavenger.

KEY WORDS: flame quenching, travelling waves, multiple solutions, radical scavenger

AMS subject classification: 80A25, 35K57, 35B32.

*Corresponding author.

1. Introduction

Until recently, the main methodology for tackling large-scale fires has involved the use of chemical flame extinguishants based on halon species. The use of such species has, however, now been banned under the Montreal Protocol in order to protect the Ozone Layer. No substitute extinguishant has yet been satisfactorily identified. Consequently it would be useful to develop an understanding of a general mechanism for flame quenching in order to aid the development of new extinguishants. The theoretical investigation of flame quenching started with Buckmaster's paper [1]. Since then, several simple models have been studied. Most of these studies of flame quenching, see [1,2,6,10,16] for example, have been concerned with heat removal through physical processes such as conduction or radiation. More recently a new idea, chemical quenching, has been introduced. In this situation a fine mist comprising a dilute solution of simple chemical salts is used. The mechanism of this inhibition is expected to arise through some endothermic process, for example through the evaporation of the water mist, and then through the catalysis of radical removal by the salt particles formed in this process. The simplest mechanism involving these steps has already been investigated by the present authors [11–13]. In the present paper we investigate a more realistic, and hence a more complicated model, which is an extension of the Zel'dovich–Liñan model [5] with an endothermic chemical process and which also includes the effects of a radical scavenger on the active combustion radicals.

In this case, the 'heat loss' process is controlled by the endothermic decomposition of an inhibitor species W leading to the formation of a 'radical scavenger' S, which acts as a catalyst for the removal of active radicals X through an additional termination step. In particular, we are concerned with determining the conditions for the establishment of constant-velocity constant-form flame structures and the dependence of the flame speed on the reaction parameters. Our model involves the chemical reactions

$$\begin{aligned}
&A \to X && \text{rate} = k_i a\, \mathrm{e}^{-E_i/RT},\\
&A + X \to 2X && \text{rate} = k_b a x\, \mathrm{e}^{-E_b/RT},\\
&X + X \to P_1 + \text{ heat} && \text{rate} = k_t x^2,\\
&W \to rS - \text{ heat} && \text{rate} = k_w w\, \mathrm{e}^{-E_w/RT},\\
&S + X \to S + P_2 && \text{rate} = k_s s x.
\end{aligned} \tag{1}$$

Here A is the reactant, X is a radical intermediate, W is an inhibitor species, S is the radical scavenger, P_1, P_2 are inert products and T is (absolute) temperature. The first three (initiation, branching and termination) steps form the Zel'dovich–Liñan model [5], with rate constants k_i, k_b, k_t. The last two steps, with rate constants k_w, k_s, represent the endothermic generation and action of a chemical

scavenger S from some precursor W. The third step has a positive exothermicity (negative reaction enthalpy) $Q_t > 0$, and the fourth step has a negative exothermicity, $Q_w < 0$. The activation energies of the corresponding steps are E_i, E_b, E_w and R is the universal gas constant. We can expect the initiation step to be a relatively slow process in the flame context and will be neglected in our model, i.e. $k_i = 0$ is assumed.

One possible interpretation of the third and fourth steps in the above mechanism is the evaporation of droplets of a solution of an ionic salt producing a dispersion of solid salt particles, which then catalyse the termination of radical species. The simple first-order, Arrhenius kinetics representation of the evaporation process is clearly a simplification, perhaps appropriate to small extents of evaporation, but may allow generic features to be revealed. The stoichiometric parameter r then would be proportional to the concentration of the salt dissolved in the droplets, with $r = 0$ corresponding to pure water.

The model equations governing our system, written in a reference frame moving with the flame, are [14–17]

$$mA'(z) = \sigma D_A A''(z) - k_b e^{-E_b/RT} A(z)X(z)\frac{\sigma^2}{\mu_X}, \tag{2}$$

$$mX'(z) = \sigma D_X X''(z) + k_b e^{-E_b/RT} A(z)X(z)\frac{\sigma^2}{\mu_A} - 2k_t X(z)^2\frac{\sigma^2}{\mu_X} - k_s S(z)X(z)\frac{\sigma^2}{\mu_S}, \tag{3}$$

$$mW'(z) = \sigma D_W W''(z) - k_w e^{-E_w/RT} W(z)\sigma, \tag{4}$$

$$mS'(z) = \sigma D_S S''(z) + rk_w e^{-E_w/RT} W(z)\frac{\sigma\mu_S}{\mu_W}, \tag{5}$$

$$mC_p T'(z) = \lambda T''(z) + Q_t k_t X(z)^2\frac{\sigma^2}{\mu_X^2} + Q_w k_w e^{-E_w/RT} W(z)\frac{\sigma}{\mu_W}, \tag{6}$$

where A, X, W, S are mass fractions of the corresponding species, m is mass flux, σ is total density, D_A, D_X, D_W, D_S are the diffusion coefficients, μ_A, μ_X, μ_W, μ_S are molar masses, C_p is the constant-pressure specifc heat and λ is thermal conductivity. Primes denote differentiation with respect to the travelling wave co-ordinate z. Equations (2–6) are subject to the boundary conditions

$$A \to A_0, \quad X \to 0, \quad W \to W_0, \quad S \to 0, \quad T \to T_a \quad \text{as } z \to -\infty, \tag{7}$$

$$A' \to 0, \quad X' \to 0, \quad W' \to 0, \quad S' \to 0, \quad T' \to 0 \quad \text{as } z \to +\infty, \tag{8}$$

where A_0 and W_0 denote the initial mass fractions of reactants A and W and T_a is the ambient temperature and are the conditions ahead of the flame.

Some aspects of kinetic system (1) were investigated using high activation energy asymptotics in [8]. The time dependent system corresponding to this model was investigated numerically in [4]. We have also considered this system in the scavenger-free case ($r = 0$) with unit Lewis numbers in [7,12], and with arbitrary Lewis numbers in [13]. In [12,13] the exothermic reaction was taken to be a first-order reaction. From these previous studies, we expect the important parameters to be α, which represents a characteristic rate at which heat is lost by the endothermic reaction relative to the rate at which it is produced by the exothermic reaction, β the rate at which the inhibitor W is consumed relative to the fuel A, ρ, which represents the fraction of radical scavenger molecules produced by the decomposition of the inhibitor W, and $\mu = E_w/2E_b$, the ratio of the activation energies.

The aim of the present work is to determine how the dimensionless flame velocity c depends on the 'heat loss' parameters α and ρ for different values of μ, β and the Lewis numbers. In particular, we wish to determine whether there are critical values of α and ρ at which flame extinction occurs. In section 3 we present our results concerning the shape of the bifurcation diagrams for c as a function of α and ρ, which will be referred to as (α, c) and (ρ, c) curves. We determine these curves by numerical integration of the dimensionless flame equations and with pseudoarclength continuation for different values of μ, β and the Lewis number. Our numerical investigation reveals that the (α, c) curves can have three different shapes depending on the values of μ, β and the Lewis number. They can be monotone decreasing or they can have one turning point or three turning points. It turns out that for suitable positive values of ρ there is a quenching value of α above which there is no flame initiation, and below which there is a range of α where there are four different flame velocities. The determination of these bifurcation curves represents a considerable advance on what we have been able to determine previously about our model [4,7,8] as here we are able to employ the powerful numerical algorithm that we have developed recently specifically for finding the steady flame solution for this and related models [10, 12,13].

In section 4 we derive a high activation energy analysis. The previous high activation energy asymptotics [8] for our model was restricted to the case when μ was small. This analysis gave rise to further multiple solutions and different qualitative behaviour of the (α, c) curves when the effect of the radical scavenger was included, $\rho \neq 0$. In this case the consumption of the fuel and inhibitor took place within the same reaction region. Removing this restriction on μ being small, separates the reaction zones, and now the heat generated by the combustion reaction uses up all the fuel before the inhibitor is consumed, with this taking place in a further reaction zone of wider extent. Our analysis gives some qualitative confirmation of our numerical results, showing the possible existence of four solution branches, though any quantitative agreement is very much dependent on the particular values of the parameters.

2. Model and theoretical results

2.1. Model

In order to make equations (2–6) dimensionless, we introduce the following variables

$$y = \xi z, \qquad a(y) = \frac{A(z)}{A_0}, \qquad x(y) = \frac{X(z)}{X_0},$$
$$w(y) = \frac{W(z)}{W_0}, \qquad s(y) = \frac{S(z)}{S_0}, \qquad b(y) = \frac{T(z) - T_a}{T_b - T_a}, \tag{9}$$

where

$$T_b = T_a + \frac{Q_t A_0}{2\sigma C_p \mu_A}, \qquad \xi^2 = \frac{\sigma C_p A_0 k_b^2}{2\lambda k_t \mu_A} \mathrm{e}^{-2E_b/RT_b},$$

$$X_0 = \frac{A_0 k_b \mu_X}{2k_t \mu_A} \mathrm{e}^{-E_b/RT_b}, \qquad S_0 = \frac{\mu_S A_0 k_b}{k_s \mu_A} \mathrm{e}^{-E_b/RT_b},$$

(T_b is burnt gas temperature). Substituting (9) into equations (2–6) and introducing the parameters

$$\varepsilon = \frac{RT_b}{2E_b}, \qquad L_A = \frac{\lambda}{D_A \sigma C_p}, \qquad L_X = \frac{\lambda}{D_X \sigma C_p},$$
$$L_W = \frac{\lambda}{D_W \sigma C_p}, \qquad L_S = \frac{\lambda}{D_S \sigma C_p}, \tag{10}$$

$$\alpha = \frac{4(-Q_w) W_0 k_t k_w \sigma \mu_A^2}{Q_t A_0^2 k_b^2 \mu_W} \mathrm{e}^{(2E_b - E_w)/RT_b}, \qquad \beta = \frac{2k_t k_w \mu_A}{A_0 k_b^2} \mathrm{e}^{(2E_b - E_w)/RT_b}, \tag{11}$$

$$c = \frac{mC_p}{\lambda \xi}, \qquad \mu = \frac{E_w}{2E_b}, \qquad \rho = r \frac{W_0 k_s \mu_A}{A_0 k_b \mu_W} \mathrm{e}^{E_b/RT_b}, \qquad \delta = \frac{k_b}{2k_t \sigma} \mathrm{e}^{-E_b/RT_b} \tag{12}$$

with the temperature dependence of the reaction rates then given by

$$f_1(b) = \mathrm{e}^{(b-1)/2\varepsilon b}, \qquad f_2(b) = \mathrm{e}^{\mu(b-1)/\varepsilon b}, \tag{13}$$

we obtain the dimensionless equations for our model as

$$L_A^{-1}a'' - c\,a' - axf_1(b) = 0, \tag{14}$$

$$\delta(L_X^{-1}x'' - c\,x') + axf_1(b) - x^2 - sx = 0, \tag{15}$$

$$L_W^{-1}w'' - c\,w' - \beta w f_2(b) = 0, \tag{16}$$

$$L_S^{-1}s'' - c\,s' + \rho\,\beta w f_2(b) = 0, \tag{17}$$

$$b'' - cb' + x^2 - \alpha w f_2(b) = 0 \tag{18}$$

on $-\infty < y < \infty$, where primes now denote differentiation with respect to y and c is the dimensionless flame velocity. Here we assume that $T_a = 0$ in order to avoid the mathematical difficulties associated with a 'cold boundary' [17]. The boundary conditions are

$$a \to 1, \qquad x \to 0, \qquad w \to 1, \qquad s \to 0, \qquad b \to 0 \qquad \text{as} \quad y \to -\infty, \tag{19}$$

$$a' \to 0, \qquad x' \to 0, \qquad w' \to 0, \qquad s' \to 0, \qquad b' \to 0 \qquad \text{as} \quad y \to \infty. \tag{20}$$

We also assume that

$$\begin{aligned} &c > 0 \quad \text{and } b(y) > 0, \quad a(y) \geqslant 0, \quad x(y) \geqslant 0, \\ &w(y) \geqslant 0, \quad s(y) \geqslant 0, \quad \text{on } -\infty < y < \infty. \end{aligned} \tag{21}$$

This assumption excludes the trivial solution $b \equiv 0$, $a \equiv 1$, $x \equiv 0$, $w \equiv 1$, $s \equiv 0$. The Lewis numbers L_A, L_X, L_W, L_S and the parameters α, β, μ, ρ, δ, ε are all non-negative.

The five-variable systems (14–18) will be reduced to a three-variable one by taking $L_S = L_W$ and δ small. Both assumptions are physically reasonable (note that in (12) δ contains a factor $\exp(-1/\varepsilon)$), and they will simplify the analysis. Multiplying equation (16), with $L_W = L_S$, by ρ, adding to (17) and integrating from $-\infty$ to $+\infty$ we obtain

$$s = \rho(1 - w) \tag{22}$$

on using boundary conditions (19, 20). This expression can be substituted into equation (15) and equation (17) can be omitted. A further reduction can be made by taking δ small. Equation (15) then gives, using (22),

$$x(af_1(b) - \rho(1 - w) - x) = 0.$$

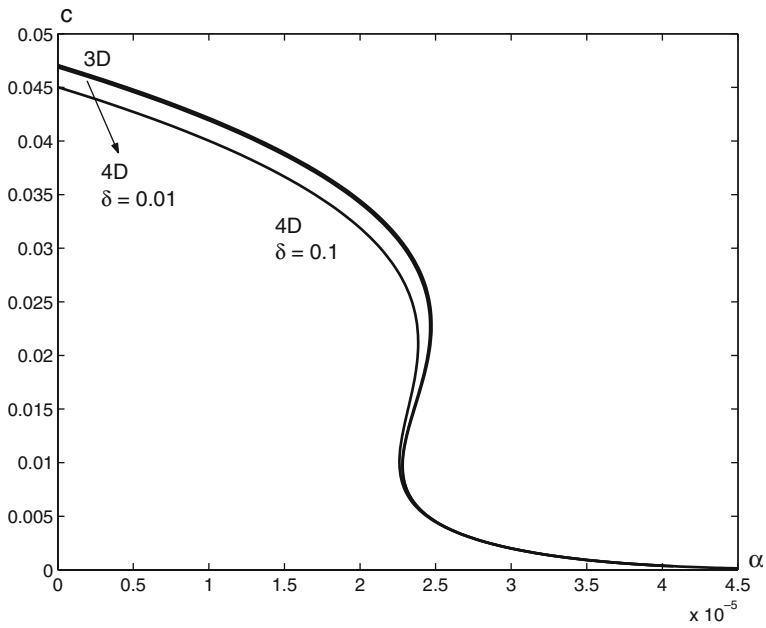

Figure 1. The (α, c) curves for $\varepsilon = 0.1$, $\beta = 0.0001$, $\mu = 0.005$, $L_A = L_W = 1$, $\rho = 0$ obtained from the three-variable system (indicated with 3D) and from the four-variable system (indicated with 4D) with $\delta = 0.1$ and $\delta = 0.01$.

Hence we put

$$x = \begin{cases} af_1(b) - \rho(1-w) & \text{if } af_1(b) - \rho(1-w) \geqslant 0, \\ 0 & \text{otherwise} \end{cases} \tag{23}$$

in equations (14) and (18). Thus the three-variable system to be solved consists of equations (14), (16) and (18), in which x is given by (23) together with boundary conditions (19, 20).

We have checked the validity of approximation (23) by solving the four-variable system (14), (15), (16), (18) with different (small) values of δ, and comparing the results to those obtained from the three-variable system. The comparison is shown in figure 1, where we plot the value of the velocity c as a function of the parameter α. The values of the other parameters are fixed, $\varepsilon = 0.1$, $\mu = 0.005$, $\beta = 0.0001$, $L_A = L_W = 1, \rho = 0$. We can see that for $\delta = 0.1$ the curves are qualitatively similar, and for $\delta = 0.01$ they are very close to each other. We note that for $\delta \leqslant 0.001$ the two curves coincide.

2.2. Theoretical results

We now derive some qualitative properties of the original five-variable system given by equations (14–18) without the simplifying assumptions $L_S = L_W$ and δ small.

Proposition 1. The function a is strictly decreasing, w is decreasing and s is increasing on $-\infty < y < \infty$. If $\beta > 0$, then w and s are also strictly monotone.

Proof. Multiplying equation (14) by $L_A e^{-L_A c y}$ and integrating over (y, ∞) we obtain

$$a'(y)e^{-L_A c y} = -L_A \int_y^\infty e^{-L_A c t} a(t) x(t) f_1(b(t)) dt$$

giving $a'(y) < 0$ for all y, because the integral is positive using (22). Similarly from equation (16) we obtain $w'(y) \leqslant 0$, and from equation (17) we obtain $s'(y) \geqslant 0$. In the case $\beta > 0$ we get $w'(y) < 0$ and $s'(y) > 0$. □

Proposition 2. The limits

$$a_+ = \lim_{y\to\infty} a(y), \quad b_+ = \lim_{y\to\infty} b(y), \quad w_+ = \lim_{y\to\infty} w(y), \quad s_+ = \lim_{y\to\infty} s(y)$$

exist

$$\lim_{y\to\infty} x(y) = 0, \tag{24}$$

$$\rho w_+ + s_+ = \rho \tag{25}$$

and

$$a_+ + b_+ - \frac{\alpha}{\beta} w_+ \leqslant 1 - \frac{\alpha}{\beta}. \tag{26}$$

Proof. The existence of a_+ and w_+ follows from (22) and the monotonicity of the functions a and w.

If $\beta = 0$, equations (16) and (17) give $w \equiv 1$ and $s \equiv 0$. If $\beta > 0$ then, from equation (16), $w f_2(b) \to 0$ as $y \to \infty$. Equation (18) then gives $x \to 0$ as $y \to \infty$. If we now integrate equation (16) and apply boundary condition (19), we find

$$c(1 - w_+) = \beta \int_{-\infty}^\infty w(y) f_2(b(y)) dy. \tag{27}$$

Hence the infinite integral in (27) exists since w_+ does. For $\rho = 0$, equation (17) gives $s \equiv 0$. With $\rho > 0$, integrating equation (17) and applying (19) gives

$$cs_+ = \rho\beta \int_{-\infty}^{\infty} w(y) f_2(b(y)) \mathrm{d}y \tag{28}$$

since on the right-hand side approaches a finite limit as $y \to \infty$. Thus s_+ exists. Adding equations (16, 17) and integrating, gives

$$\rho(L_W^{-1} w' - cw) + (L_S^{-1} s' - cs) = -\rho c. \tag{29}$$

Applying the above limits in (29) gives the result (25).

To establish the existence of b_+ and derive (26) we combine equations (14–16) and (18) to eliminate reaction terms, integrate on $(-\infty, y)$ and apply boundary conditions (19)

$$L_A^{-1} a' - c(a-1) + \delta(L_X^{-1} x' - cx) + \frac{\alpha}{\beta}(c(w-1) - L_W^{-1} w') + b' - cb = \int_{-\infty}^{y} s(t) x(t) \mathrm{d}t. \tag{30}$$

Since all the terms in (30) have finite limits as $y \to \infty$ apart from cb, taking this limit shows that b_+ exists. Using the fact that on the right-hand side of (30) and c are both non-negative, (22) yields (26). □

We will refer to the case $\alpha = \rho = 0$ as the 'adiabatic case', since there is no heat loss from the system. In this case (14–18) reduces to a system of three equations, and assuming $\delta = 0$ we get the usual equations of the adiabatic case. In [9] it was shown that this system has a unique solution when $L_A \geqslant 1$, i.e. there exists a unique value of c for which this problem has a solution. This value of c will be denoted by c_{ad}. (In the case $L_A < 1$ uniqueness has not been proved, nevertheless, in the numerics the adiabatic velocity c_{ad} appears to be unique for this case as well.)

3. Numerical results

Here we present our numerical results obtained by the finite-difference discretisation of our reduced three-variable boundary-value problem:

$$L_A^{-1} a'' - c\, a' - a x f_1(b) = 0 \tag{31}$$

$$L_W^{-1} w'' - c\, w' - \beta w f_2(b) = 0 \tag{32}$$

$$b'' - cb' + x^2 - \alpha w f_2(b) = 0 \tag{33}$$

$$a \to 1, \quad w \to 1, \quad b \to 0 \quad \text{as} \quad y \to -\infty, \tag{34}$$

$$a' \to 0, \quad w' \to 0, \quad b' \to 0 \quad \text{as} \quad y \to \infty, \tag{35}$$

where x is given by (23). In order to determine the number of solutions for different values of the parameters α, ρ, μ, β, L_A, L_W, we plot the value of c versus α and ρ, when the values of the other parameters are fixed. We will refer to these curves, respectively, as (α, c) and as (ρ, c) curves. These curves are obtained using a pseudoarclength continuation method [3]. Our numerical method was described fully in [12], where we considered the case $\rho = 0$ with unit Lewis numbers $L_A = L_W = 1$, in which case the system can be reduced to two equations.

As in [12] we introduce the new independent variable $\overline{y} = cy$ and then approximate problem (31–35) with a boundary-value problem on a bounded interval $[0, L]$. The approximation is based on the fact that the non-linear (reaction) terms tend to zero as $y \to \pm\infty$. Neglecting the non-linear terms in $(-\infty, 0)$ and in (L, ∞) the differential equations can be solved analytically in these regions, hence we get boundary conditions for all three functions at $\overline{y} = 0$ and at $\overline{y} = L$, ensuring the smoothness of the solution. Using the translational invariance of the differential equations we can assume that $b(0) = b_I$, where b_I is a suitably chosen small number, corresponding to an ignition temperature. This gives seven undetermined boundary conditions. The extra boundary condition is used to determine the value of the velocity c.

Introducing N grid points in the interval $[0, L]$, we discretise the differential equations with finite differences, giving $3(N-2)$ equations at the internal grid points. Hence, together with the seven boundary conditions we have $3N+1$ equations for the same number of unknowns. This system can be solved using Newton–Raphson iteration if a good initial guess is known. The solution for the adiabatic case $\alpha = \rho = 0$ can be obtained easily starting from linear profiles as an initial guess. Then, increasing the value of α or ρ, the solution can be obtained by continuation using a standard pseudoarclength continuation method [3]. We also considered the values of b_I and L to ensure that problem given in $[0, L]$ is a good approximation to (31–35). It turned out that $L = 10$ and $b_I = 0.1$ was suitable for most of the parameter range considered.

In our numerical studies we fixed the value of ε at $\varepsilon = 0.1$ and determined the (α, c) and (ρ, c) curves for different values of L_A, L_W, μ and β. We found, that the characterization of these curves is based on the classification of the (α, c) curves for the $\rho = 0$ case given in [12]. Therefore we briefly recall this classification. The (α, c) curve could have three different shapes depending on the value of μ and β. For $\mu > 1$ the curve was monotone decreasing with increasing α and was unbounded in the α direction, i.e. there was no quenching. For $\mu \leqslant 1$ the curve was bounded in the α direction, with $c \to 0$ at a finite value of α, and had two different shapes. For larger values of β the curve was monotone decreasing and for smaller values of β it was S-shaped. These results suggest that, for $\mu < 1$, hysteresis bifurcations occur at certain values of β. The parameter pair (μ, β) is a hysteresis bifurcation point if the (α, c) curve has an inflexion. The hysteresis bifurcation curve was determined in [12]

for $L_A = L_W = 1$, and for general Lewis numbers in [13]. It was found that, by increasing the value of L_A, the hysteresis bifurcation curve in the (μ, β) parameter plane moved to the left. If the (μ, β) parameter pair was above the curve, then the (α, c) curve was decreasing and bounded. If it was below the curve, then the (α, c) curve was S-shaped. The hysteresis bifurcation curve appeared to tend to the vertical line $\mu = 1$, though this upper limit was left unresolved in [12].

Returning to the present case, we found that the shapes of the (α, c) and (ρ, c) curves are determined by the position of the (μ, β) parameter pair with respect to the $\mu = 1$ line and to corresponding the hysteresis bifurcation curve. These curves divide the (μ, β) parameter plane into three regions. In the course of our numerical study we fixed the value of the Lewis numbers and, choosing a (μ, β) parameter pair, we first determined the flame velocity and the profiles for the adiabatic case $\alpha = 0$, $\rho = 0$. Then, using the pseudoarclength continuation method starting from the adiabatic case, we determined the (α, c) curve for $\rho = 0$, and the (ρ, c) curve for $\alpha = 0$. Finally, from selected points of the (α, c) curve, we started a continuation in ρ yielding (ρ, c) curves for different values of α. Similarly, from some points of the (ρ, c) curve we started a continuation in α yielding (α, c) curves for different values of ρ. The results of these continuations are shown in figures 2–4. In these figures we also show the critical points of the (α, c) and (ρ, c) curves, i.e. the saddle-node bifurcation curves in the (α, ρ) parameter plane. These curves divide the (α, ρ) parameter plane according to the number of flame solutions. The number of solutions are also shown in the different regions.

In figure 2, for $\mu = 0.001$, $\beta = 0.0001$, we see a typical situation for the S-shaped case when the (μ, β) parameter pair is below the hysteresis bifurcation curve. From figure 2(a) we can see that $\rho = 0$ is a singular limit, as the curve for $\rho = 0$ has two turning points and increases to its large upper bound in α as $c \to 0$, whereas the curves for small positive values of ρ have three turning points, with an upper bound in α at a non-zero value of c, and return to the $\alpha = 0$ axis. Hence, for given values of the parameters there can be four solutions. At a particular value of ρ the two lower turning points merge and for larger ρ values the (α, c) curve has only one turning point. Finally, there is a critical value of $\rho = \rho_{\text{crit}}$ where the (α, c) curve disappears. The value of ρ_{crit} can be determined from the (b) part of the figure, namely it is the ρ value at the turning point of the curve for $\alpha = 0$. The evolution of the (ρ, c) curves plotted in figure 2b) shows that, for the smaller values of α, they follow the $\alpha = 0$ case with one turning point and a critical value of ρ for the existence of a steady flame. For increased values of α, there is a hysteresis bifurcation on the lower solution branch, with then two turning points appearing. On increasing α further, the branches of the (ρ, c) curves become disjoint before finally disappearing altogether at critical values of α given by the turning points on the $\rho = 0$ curve in figure 2(a). Figure 2(c) shows the saddle-node bifurcation curves, i.e. the loci of the turning points, in the (α, ρ) parameter plane. The long curve, connecting the two axes, is the locus of the turning points of the (ρ, c) curves, i.e. the curve gives the critical value

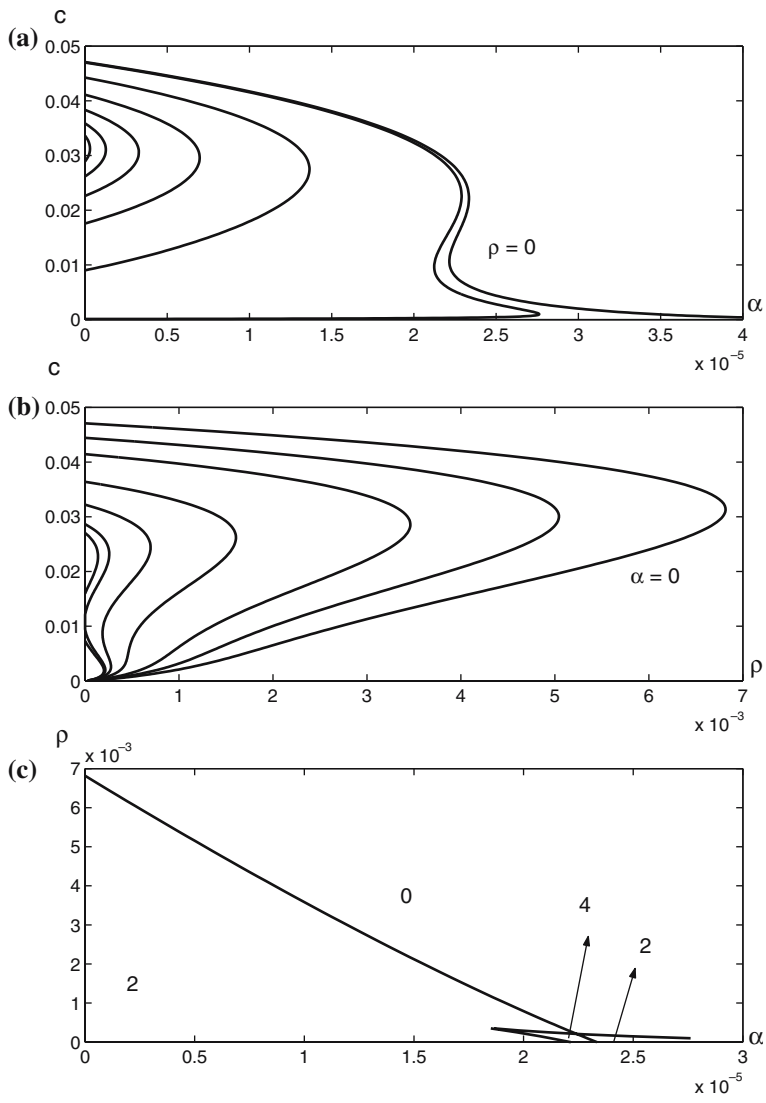

Figure 2. (a) The (α, c) curves for seven different values of ρ: $\rho = 0$, 0.0001, 0.0025, 0.0045, 0.0057, 0.0064, 0.0067. (b) The (ρ, c) curves for seven different values of α: $10^4\alpha = 0$, 0.0534, 0.1040, 0.1688, 0.2038, 0.2221, 0.2273. (c) Saddle-node bifurcation curves in the (α, ρ) parameter plane. The number of solutions is indicated in the different regions. In all the three cases $\varepsilon = 0.1$, $\mu = 0.001$, $\beta = 0.0001$, $L_A = L_W = 1$.

of the (ρ, c) curve for a given value of α, at the same time it is the locus of the upper turning points of the (α, c) curves. The critical α values at the lower two turning points of the (α, c) curve are given by the cusp curve. The left branch of the curve corresponds to the lowest turning points (maximum points), the right

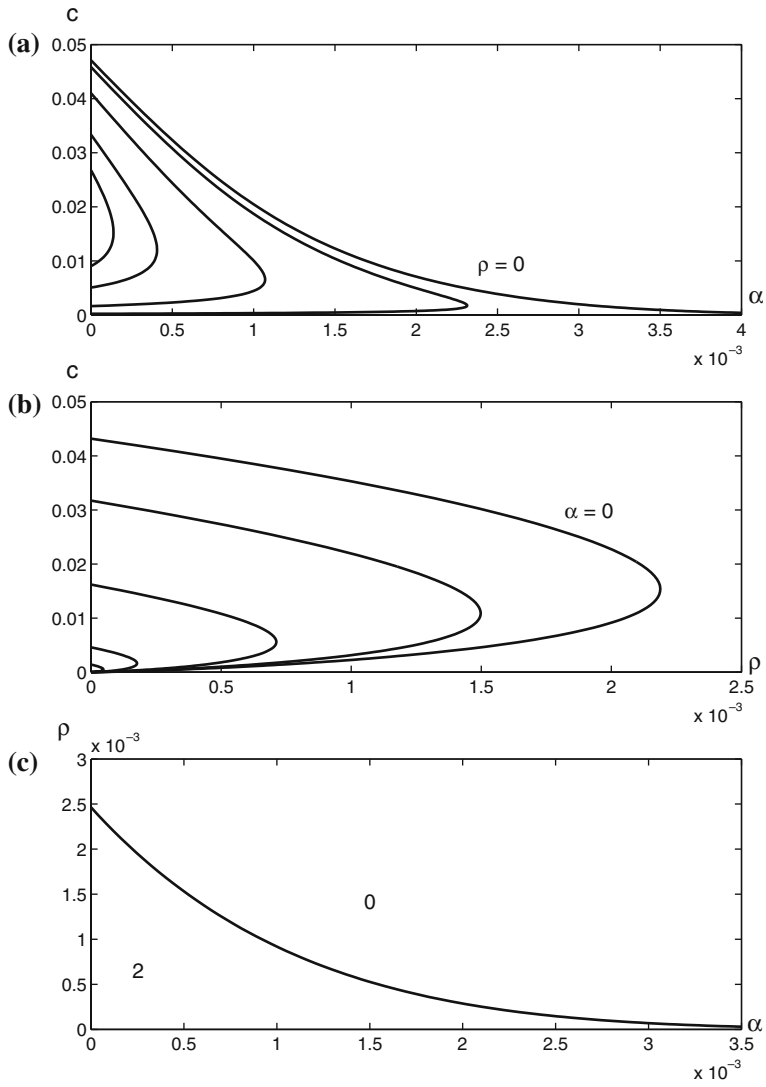

Figure 3. (a) The (α, c) curves for five different values of ρ: $\rho = 0,\ 0.0001,\ 0.0006, 0.0016,\ 0.0021$. (b) The (ρ, c) curves for five different values of α: $\alpha = 0,\ 0.0004,\ 0.0008, 0.0012,\ 0.0017$. (c) Saddle-node bifurcation curve in the (α, ρ) parameter plane. The number of solutions is indicated in the different regions. In all the three cases $\varepsilon = 0.1$, $\mu = 0.1$, $\beta = 0.01$, $L_A = L_W = 1$.

branch belongs to the middle turning points (minimum points). The numbers in the figure indicate the number of solutions in the different domains. We can see that the number of solution changes by two on both curves, as expected for saddle-node bifurcation curves.

In figure 3 we see a typical situation for the monotone, bounded case, that is when the (μ, β) parameter pair is above the hysteresis bifurcation curve, here $\mu = 0.1$, $\beta = 0.01$. In figure 3a we can see that $\rho = 0$ is again a singular limit, as the curve for $\rho = 0$ has no turning point, but the curves (small) positive values of ρ do have turning points. For the critical value of $\rho = \rho_{\text{crit}}$ the (α, c) curve disappears. The value of ρ_{crit} can be determined from the (b) part of the figure, namely it is the ρ value of the turning point of the curve for $\alpha = 0$. The (ρ, c) curves are shown in figure 3(b). All the curves for the different values of α have one turning point, with again a critical value of ρ for existence. Figure 3(c) shows the saddle-node bifurcation curve, i.e. the locus of the turning points, in the (α, ρ) parameter plane.

In figure 4 we see a typical situation for the monotone, unbounded case, $\mu = 1.5$, $\beta = 0.01$. From figure 5(a) we see that, for $\rho = 0$ and for small positive values of ρ, the curves are monotone and unbounded. However, the curves for larger values of ρ have a turning point. For the critical value of $\rho = \rho_{\text{crit}}$ the (α, c) curve again disappears at the ρ value for the turning point in the $\alpha = 0$ curve. The (ρ, c) curves are shown in figure 4(b). All the curves for different values of α have one turning point. In this case the (ρ, c) curves are not 'nested' inside each other for increasing α as they are in figures 2(b) and 3(b). The value of c for $\rho = 0$ decreases and ρ_{crit} increases as α increases. Figure 4(c) shows the saddle-node bifurcation curve.

We also investigated the effect of the Lewis numbers. In [13] we found that, in the $\rho = 0$ case, the value of L_W does not change the (α, c) curve significantly. Some numerical experiments suggest that this is the same in the $\rho > 0$ case as well. However, we did not perform a systematic numerical investigation for different values of L_W. Instead we used the physically relevant assumption $L_A = L_W$ in determining the (α, c) and (ρ, c) curves. For different values of L_A we repeated the numerical experiments shown in figure 2–4 and found that the (α, c) and (ρ, c) curves can have the same shapes as for unit Lewis numbers. Our results are summarised in figure 5, where $\mu = 0.005$ and $\beta = 10^{-4}$ are fixed and $L_A = L_W$ is changed (the values of $L_A = L_W$ are shown in the figure). In figure 5(a) the (α, c) curve is shown for $\rho = 10^{-4}$. We can see that for values $L_A > 1$ the three turning points survive, becoming more obvious, and that the value of α_{crit} increases with L_A. For values of $L_A < 1$ the two upper turning points can merge and the curve has only one turning point, with a decreased value of α_{crit}. In figure 5(b) the (ρ, c) curve is shown for $\alpha = 0$. There does not appear to be a qualitative change in the shape of the curve as L_A is changed, though the values ρ_{crit} increase considerably with L_A.

In figure 6 we show the temperature and concentration profiles in a case when there are four solutions for the same value of the parameters. The case shown in the figure is for the parameter values used for the second curve shown in figure 2(a), namely $\mu = 0.001$, $\beta = 10^{-4}$, $\rho = 10^{-4}$, and for $\alpha = 2.2 \times 10^{-5}$ there are four solutions, the corresponding values of c are shown in figure 6. We

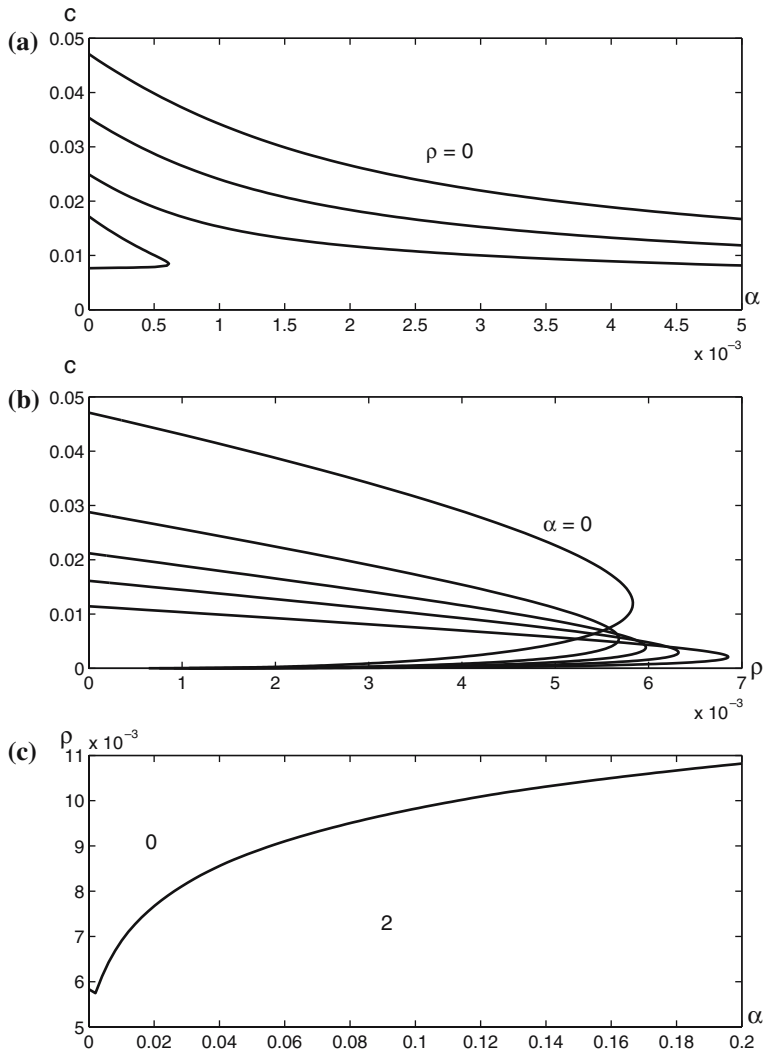

Figure 4. (a) The (α, c) curves for four different values of ρ: $\rho = 0,\ 0.0013,\ 0.0039,\ 0.0052$. (b) The (ρ, c) curves for five different values of α: $\alpha = 0,\ 0.0003,\ 0.0013,\ 0.0026,\ 0.0029$. (c) Saddle-node bifurcation curve in the (α, ρ) parameter plane. The number of solutions is indicated in the different regions. In all the three cases $\varepsilon = 0.1$, $\mu = 1.5$, $\beta = 0.01$, $L_A = L_W = 1$.

notice that the maximum temperature and the maximum value of x decreases with decreasing c. We observe that, for larger flame velocities, the fuel is consumed faster than the endothermic species w, however, for small values of c the endothermic species w is consumed first.

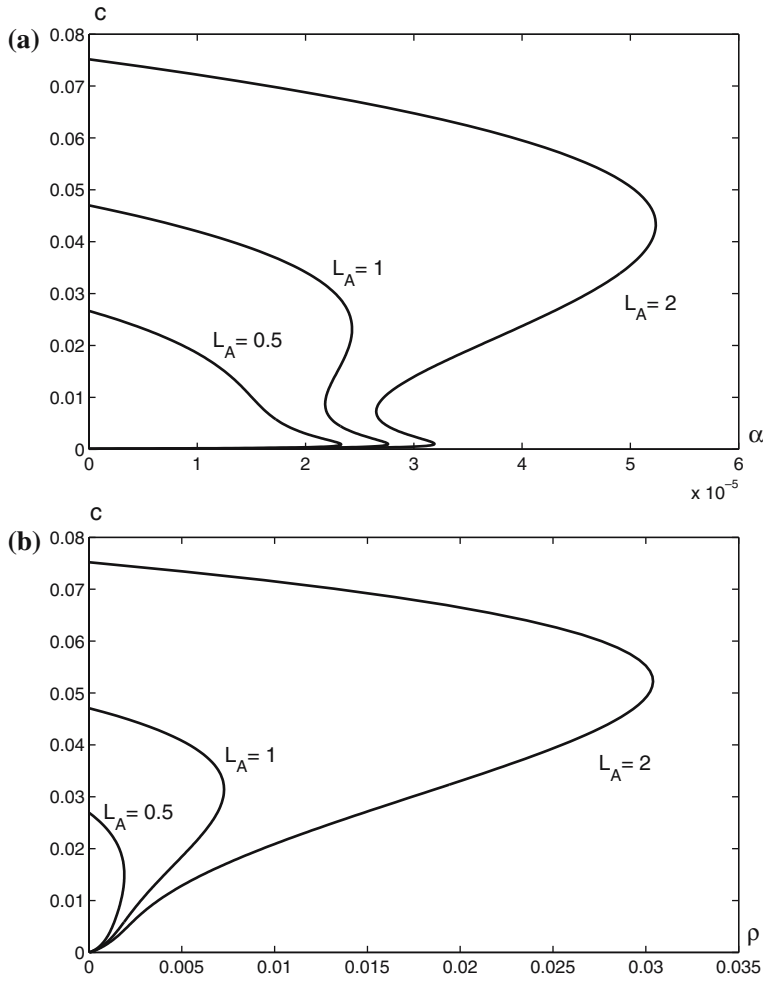

Figure 5. (a) The (α, c) curves for three different values of L_A in the case $\rho = 0.0001$. (b) The (ρ, c) curves for three different values of L_A in the case $\alpha = 0$. In both cases $\varepsilon = 0.1$, $\mu = 0.005$, $\beta = 0.0001$, $L_W = L_A$.

The above numerical solutions show that complex bifurcation behaviour is seen when α, β and ρ are small (see figure 2). We now examine this case in the high activation energy, small ε, limit.

4. High activation energy analysis

Here we obtain a solution of equations (31–33) valid in the limit as $\varepsilon \to 0$, with

$$\alpha = \varepsilon^4 \overline{\alpha}, \qquad \beta = \varepsilon^3 \overline{\beta}, \qquad \rho = \varepsilon^2 \overline{\rho}, \qquad c = \varepsilon^{3/2} \overline{c}, \tag{36}$$

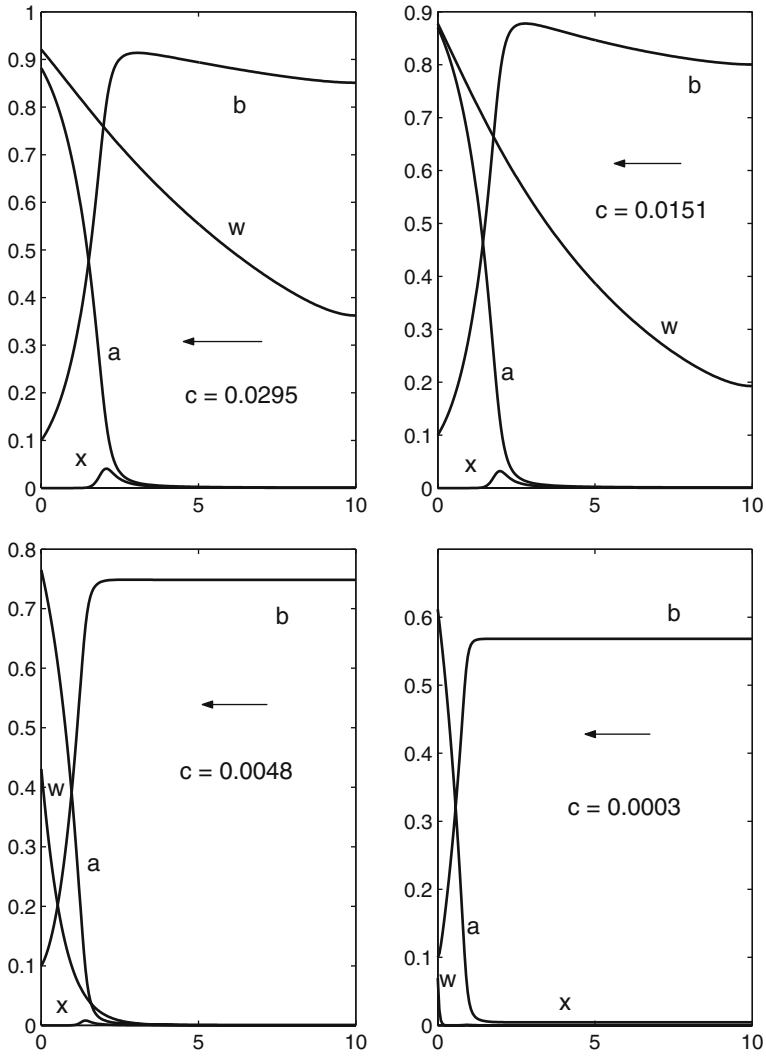

Figure 6. The temperature and concentration profiles for $\mu = 0.001$, $\beta = 10^{-4}$, $L_A = L_W = 1$, $\rho = 10^{-4}$ and for $\alpha = 2.2 \times 10^{-5}$. For these values of the parameters there are four solutions, the corresponding values of c are shown in the Figure. The direction of flame propagation is shown by the arrows.

where $\overline{\alpha}$, $\overline{\beta}$, $\overline{\rho}$, $\overline{c}$ are all of $O(1)$ as $\varepsilon \to 0$. The scaling of the flame speed c is required for consistency in the matching process that arises in the asymptotic analysis and we take $\overline{\beta} > 0$ (see proposition 2).

An equivalent case, without the inclusion of the radical scavenger and with the exothermic reaction being first-order, has been treated in [12] for unit Lewis numbers. The present case (with the effects of the scavenger included) has been

treated in [8], again for unit Lewis numbers and on the stricter assumption that μ was small, of $O(\varepsilon)$. This case has a qualitatively different asymptotic structure to that required here (and seen in [12]) and gives a less complex bifurcation behaviour. We do not make this assumption and consider the case when μ (and the Lewis numbers) are of $O(1)$.

The asymptotic structure in the present case follows that described in [12]. There is a preheat zone at the front of the flame, of thickness $O(\varepsilon^{-3/2})$, and two reaction zones. In the first zone, of thickness $O(\varepsilon^{-1/2})$, the fuel is consumed with the concentration of the inhibitor W remaining constant (to leading order). It is in the second reaction zone, of thickness $O(\varepsilon^{-3/2})$, that W reacts. We start our solution in the preheat zone, where we write $\overline{y} = \varepsilon^{3/2} y$. Since μ is $O(1)$ and $b < 1$ in this region, the (Arrhenius) reaction terms are neglible. Equation (23) then gives $x \equiv 0$ in the preheat zone. A solution is sought by expanding

$$\overline{c}(\varepsilon) = c_0 + \varepsilon c_1 + \cdots \tag{37}$$

$$\begin{aligned} a(\overline{y};\varepsilon) &= a_0(\overline{y}) + \varepsilon a_1(\overline{y}) +, \cdots, \\ b(\overline{y};\varepsilon) &= b_0(\overline{y}) + \varepsilon b_1(\overline{y}) + \cdots, \\ w(\overline{y};\varepsilon) &= w_0(\overline{y}) + \varepsilon w_1(\overline{y}) + \cdots. \end{aligned} \tag{38}$$

A straightforward calculation gives, following [12],

$$b_0 = \mathrm{e}^{c_0\overline{y}}, \qquad b_1 = (T_1 + c_1\overline{y})\,\mathrm{e}^{c_0\overline{y}}, \tag{39}$$

$$a_0 = 1 - \mathrm{e}^{L_A c_0\overline{y}}, \qquad a_1 = -c_1 L_A \overline{y}\,\mathrm{e}^{L_A c_0\overline{y}}, \tag{40}$$

$$w_0 = 1 - S_1\,\mathrm{e}^{L_W c_0\overline{y}}, \qquad w_1 = -L_W c_1 S_1 \overline{y}\,\mathrm{e}^{L_W c_0\overline{y}} + S_2\,\mathrm{e}^{L_W c_0\overline{y}}, \tag{41}$$

where the constants T_1 and S_1 will be determined in the analysis. The a_i, b_i, w_i have been chosen to satisfy the outer boundary conditions (34) and have a_0 small and $b_0 \simeq 1$ for $\overline{y}$ small. This anticipates the matching with the first reaction zone, which is what we consider next.

In this first reaction zone, where all the fuel A will be consumed, we transform equations (31–33) by putting

$$a = \varepsilon A, \qquad b = 1 - \varepsilon B, \qquad x = \varepsilon X, \qquad \zeta = \varepsilon^{1/2} y \tag{42}$$

and leaving w unscaled. We look for a solution of the resulting equations by expanding

$$\begin{aligned} A &= A_0 + \varepsilon A_1 + \cdots, \quad & B &= B_0 + \varepsilon B_1 + \cdots, \\ X &= X_0 + \varepsilon X_1 + \cdots, \quad & w &= w_0 + \varepsilon w_1 + \cdots. \end{aligned} \tag{43}$$

On using (36) and (37), we obtain, at leading order, from (23),

$$X_0 = A_0 \, \mathrm{e}^{-B_0/2}. \tag{44}$$

Applying (44) in equations (31) and (33) then gives

$$L_A^{-1} A_0'' - A_0^2 \, \mathrm{e}^{-B_0} = 0, \qquad B_0'' - A_0^2 \, \mathrm{e}^{-B_0} = 0 \tag{45}$$

(where primes denote differentiation with respect to ζ). The matching conditions are, from (39,40), that

$$A_0 \sim -c_0 L_A \zeta, \qquad B_0 \sim -c_0 \, \zeta - T_1, \qquad \text{as} \quad \zeta \to -\infty \tag{46}$$

We can eliminate the reaction terms from equations (45) and, on integrating and applying the matching conditions (46), we find that

$$L_A^{-1} A_0 = B_0 + T_1. \tag{47}$$

Using (47) in equation (45), integrating and applying (46) gives

$$B_0'^2 = c_0^2 - 2L_A^2((B_0 + T_1)^2 + 2(B_0 + T_1) + 2) \, \mathrm{e}^{-B_0}. \tag{48}$$

As $\zeta \to \infty$, $A_0 \to 0$ (all fuel consumed), so that $B_0 \to -T_1$. Equation (48) then gives, in this limit,

$$c_0^2 = 4L_A^2 \, \mathrm{e}^{T_1}. \tag{49}$$

Equations (32) and (41) give, at leading order,

$$w_0'' = 0, \qquad w_0 \to 1 - S_1 \quad \text{as} \quad \zeta \to -\infty \tag{50}$$

so that $w_0 \equiv 1 - S_1$.

At $O(\varepsilon)$, we have, from (23,31,33), that

$$X_1 = \mathrm{e}^{-B_0/2} \left(A_1 - \frac{A_0}{2}(B_1 + B_0^2) \right) - \overline{\rho} \, (1 - S_1) \tag{51}$$

and

$$L_A^{-1} A_1'' - c_0 A_0' - \mathrm{e}^{-B_0/2} \left(A_0 X_1 + A_1 X_0 - \frac{A_0 X_0}{2}(B_1 + B_0^2) \right) = 0,$$
$$B_1'' - c_0 B_0' - 2X_0 X_1 = 0. \tag{52}$$

We can eliminate X_0 and X_1 from equations (52) using (44,51). Combining the resulting equations then gives

$$B_1'' - c_0 B_0' - (L_A^{-1} A_1'' - c_0 A_0') + \overline{\rho} \, (1 - S_1) L_A (B_0 + T_1) \, \mathrm{e}^{-B_0/2} = 0 \tag{53}$$

The matching conditions are, from (39, 40), that

$$B_1 \sim -\frac{c_0^2}{2}\zeta^2 - (c_1 + c_0 T_1)\zeta + \cdots,$$
$$A_1 \sim -\frac{L_A^2 c_0^2}{2}\zeta^2 - c_1 L_A \zeta + \cdots \quad \text{as } \zeta \to -\infty \tag{54}$$

If we integrate equation (53) and apply the matching conditions (46,54), we obtain

$$B_1' - c_0 B_0 - (L_A^{-1} A_1' - c_0 A_0) + \overline{\rho}(1 - S_1) L_A \int_{-\infty}^{\zeta} (B_0 + T_1)\, \mathrm{e}^{-B_0/2} \mathrm{d}\overline{\zeta} = 0. \tag{55}$$

Equation (55) gives, on letting $\zeta \to \infty$,

$$B_1 \sim -(c_0 T_1 + \overline{\rho}(1 - S_1) I_1)\, \zeta + \cdots \quad \text{as} \quad \zeta \to \infty \tag{56}$$

since $A_1 \to 0$, where I_1 is the integral [8]

$$I_1 = L_A \int_{-\infty}^{\infty} (B_0 + T_1) \mathrm{e}^{-B_0/2} \mathrm{d}\zeta = \int_0^{\infty} \frac{s \mathrm{e}^{-s/2}}{\sqrt{4 - 2(s^2 + 2s + 2)\mathrm{e}^{-s}}} \mathrm{d}s = 4.9283$$

on using (48,49).

Equation (32) and (41) give

$$L_W^{-1} w_1'' - c_0 w_0' = 0, \quad w_1 \sim -S_1 L_W c_0 \zeta + S_2 \quad \text{as} \quad \zeta \to -\infty. \tag{57}$$

From which it follows that $w_1 = -S_1 L_W c_0 \zeta + S_2$.

We are now in a position to consider the second reaction region (for W). In this region $a \equiv 0$ and hence, from (23), $x \equiv 0$. The behaviour of b and w as $\zeta \to \infty$ suggests a scaling for this region of

$$b = 1 - \varepsilon U, \qquad Y = \varepsilon^{3/2} y \tag{58}$$

with w left unscaled. Applying (58) in equations (32) and (33) gives, for the leading order terms (U_0, w_0) in an expansion in powers of ε,

$$U_0'' - c_0 U_0' + \overline{\alpha}\, w_0\, \mathrm{e}^{-\mu U_0} = 0, \tag{59}$$

$$L_W^{-1} w_0'' - c_0 w_0' - \overline{\beta}\, w_0\, \mathrm{e}^{-\mu U_0} = 0, \tag{60}$$

(where primes now denote differentiation with respect to Y), subject to the matching conditions

$$U_0 \sim -T_1 - (c_0 T_1 + \overline{\rho}(1 - S_1) I_1) Y + \cdots, \tag{61}$$
$$w_0 \sim (1 - S_1) - S_1 L_W c_0 Y + \cdots \quad \text{as} \quad Y \to 0.$$

On eliminating the reaction terms from equations (59) and (60), integrating and applying the matching conditions (61), we obtain

$$\overline{\beta}(U_0' - c_0 U_0) + \overline{\alpha}(L_W^{-1} w_0' - c_0 w_0) = -\overline{\alpha} c_0 - \overline{\rho}\overline{\beta} I_1 (1 - S_1). \tag{62}$$

The leading order problem is then given by equations (59) and (62) subject to the boundary conditions given by (61) and that

$$U_0' \to 0, \quad w_0 \to 0 \quad \text{as} \quad Y \to \infty \tag{63}$$

with T_1 related to c_0 by equation (49). A (numerical) solution of this system determines S_1 and T_1 in terms of c_0 and hence the corresponding $(\overline{\alpha}, c_0)$ or $(\overline{\rho}, c_0)$ curves can be found.

We can obtain the solution directly, when $\overline{\alpha} = 0$. From (59) and (61), $U_0 = -T_1$ (a constant) in this case, with then

$$T_1 = -\frac{\overline{\rho} I_1 (1 - S_1)}{c_0}. \tag{64}$$

Equation (60) can be solved to give, on applying the matching conditions (61),

$$w_0 = \frac{L_W c_0}{\gamma + L_w c_0} \mathrm{e}^{-\gamma Y}, \quad \text{where } \gamma = \frac{1}{2}\left(\sqrt{L_W^2 c_0^2 + 4\overline{\beta} L_W \mathrm{e}^{\mu T_1}} - L_W c_0\right),$$
$$S_1 = \frac{\gamma}{\gamma + L_W c_0}. \tag{65}$$

Applying (64) in (65) gives an equation for $\overline{\rho}$ in terms of T_1 as

$$\overline{\rho} = -\frac{1}{L_W I_1} T_1 \mathrm{e}^{T_1/2}\left(L_A L_W + \sqrt{L_W^2 L_A^2 + \overline{\beta} L_W \mathrm{e}^{(\mu-1)T_1}}\right). \tag{66}$$

From (66) we must have $T_1 \leqslant 0$, with $\overline{\rho} = 0$ at $T_1 = 0$ ($c_0 = 2L_A$) and $\overline{\rho} \to 0$ as $T_1 \to -\infty$ ($c_0 \to 0$) with $\overline{\rho} > 0$ in this range. Thus there is at least one turning point on $-\infty < T_1 < 0$ giving critical values for $\overline{\rho}$ when $\overline{\alpha} = 0$. This can be seen in the numerical solutions, see figures 2(b), 3(b), 4(b) and 5(b).

For $\mu = 1$, $T_{1,\mathrm{crit}} = -2$ and hence

$$\overline{\rho}_{\mathrm{crit}} = \frac{2\mathrm{e}^{-1}}{L_W I_1}\left(L_W L_A + \sqrt{L_W^2 L_A^2 + \overline{\beta} L_W}\right) \tag{67}$$

showing that there is only one turning point in this case. For $\mu \neq 1$ it is possible to have three turning points and hence four solution branches. To investigate this possibility we differentiate $\overline{\rho}$ in expression (66) with respect to T_1 and, on equating this to zero, we find after a little algebra that the turning points of (66) are found where

$$L_A L_W\left(L_A L_W + \sqrt{L_W^2 L_A^2 + \overline{\beta} L_W \mathrm{e}^{(\mu-1)T_1}}\right) = -\frac{\overline{\beta} L_W \mathrm{e}^{(\mu-1)T_1}(\mu T_1 + 2)}{(T_1 + 2)}. \tag{68}$$

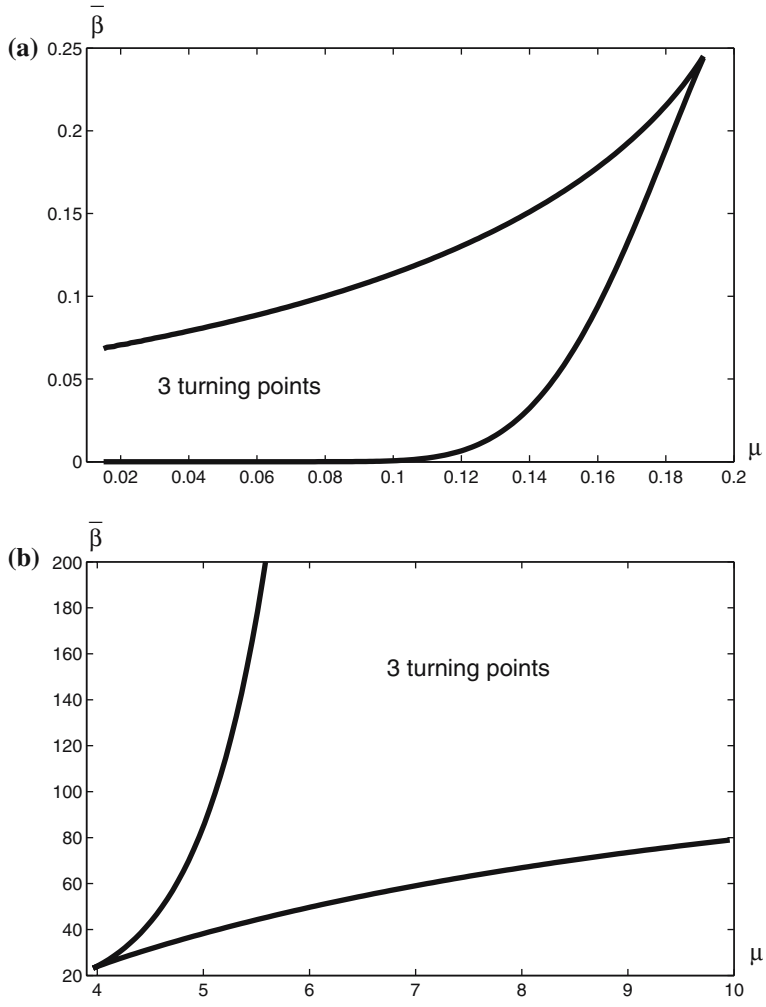

Figure 7. The $\overline{\beta} - \mu$ parameter plane, showing the region where three turning points (four solution branches) can occur in expression (66) for $\overline{\alpha} = 0$, (a) small μ, (b) large μ, $L_A = L_W = 1$.

Since on the left-hand side of (68) is positive and monotone for all T_1, the turning points of (66) must lie in the range

$$-2 < T_1 < -\frac{2}{\mu} \quad \text{for} \quad \mu > 1, \qquad -\frac{2}{\mu} < T_1 < -2 \quad \text{for} \quad \mu < 1. \tag{69}$$

For (66) to have more than one turning point, on the right-hand side of (68) must also have turning points. These arise where

$$\mu(T_1 + 2)^2 - 2(\mu - 1)(T_1 + 2) + 2 = 0, \tag{70}$$

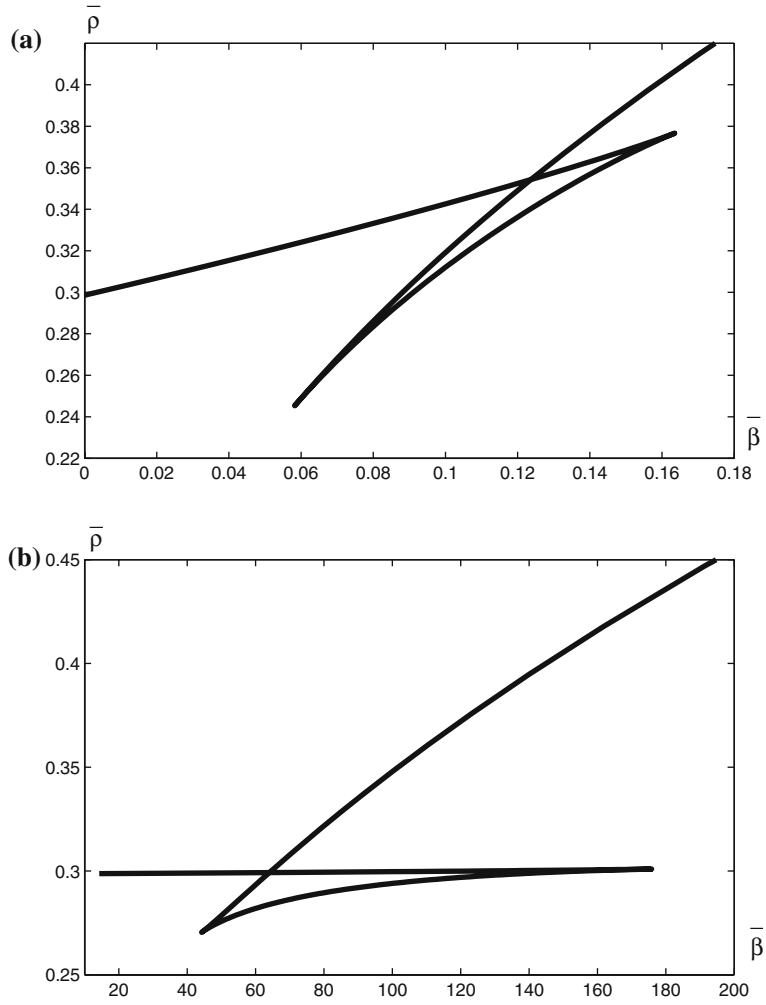

Figure 8. The positions of the saddle-node bifurcations in the $\overline{\rho}$ – $\overline{\beta}$ plane for (a) $\mu = 0.15$, (b) $\mu = 5.5$.

which gives a necessary condition for the existence of three turning points that

$$\mu < 2 - \sqrt{3} \quad \text{or} \quad \mu > 2 + \sqrt{3}, \tag{71}$$

when condition (71) is satisfied both roots of equation (70) satisfy conditions (69). The final requirement for multiple solutions is that the local maximum and the local minimum on the right-hand side of equation (68), given by the values of T_1 obtained from (70), must, respectively, lie above and below the curve given by on the left-hand side of equation (68).

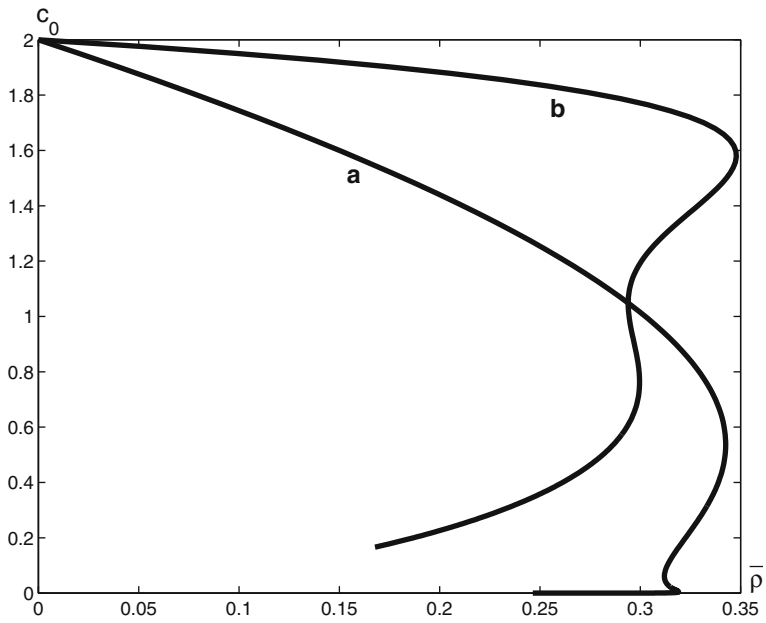

Figure 9. The existence of four solutions to equation (66). Plots of c_0 against $\overline{\rho}$ for $L_A = L_W = 1.0$ and (a) $\overline{\beta} = 0.1$, $\mu = 0.15$, (b) $\overline{\beta} = 100.0$, $\mu = 5.5$.

We can use (68,69,71) to map out the $\overline{\beta}$ – μ parameter plane in which there are three turning points. The results are shown in figure 7 for $L_A = L_W = 1.0$, with $\mu > 3.96$ or $\mu < 0.191$ being necessary for four solution branches, slightly less or greater values respectively than given by (71). Figure 7 enables us to determine, for a given value of μ, the curves in the $\overline{\rho}$ – $\overline{\beta}$ parameter plane on which the turning points in the c_0 – $\overline{\rho}$ plots occur. These are illustrated in figure 8 for $\mu = 0.15$ and $\mu = 5.5$. The cusp points on these curves are given by the values for $\overline{\beta}$ at $\mu = 0.15$ and at $\mu = 5.5$ in figure 7. The corresponding c_0 – $\overline{\rho}$ plots are shown in figure 9 for $\overline{\beta} = 0.1$ and for $\overline{\beta} = 100.0$. For these parameter values the turning points are at, respectively, $(c_0, \overline{\rho}) = (0.061, 0.312)$, $(0.014, 0.318)$, $(0.538, 0.343)$ and at $(c_0, \overline{\rho}) = (1.046, 0.294)$, $(0.764, 0.300)$, $(1.581, 0.348)$.

We now assume that $\overline{\alpha} > 0$. In the case when $L_W = 1$ we can integrate equation (62) again, following [12], to get

$$\overline{\beta} U_0 + \overline{\alpha} w_0 = \overline{\alpha} + \frac{\overline{\rho}\overline{\beta} I_1 (1 - S_1)}{c_0} \tag{72}$$

from which it follows that

$$\overline{\beta} T_1 + \overline{\alpha} S_1 = -\frac{\overline{\rho}\overline{\beta} I_1 (1 - S_1)}{c_0}. \tag{73}$$

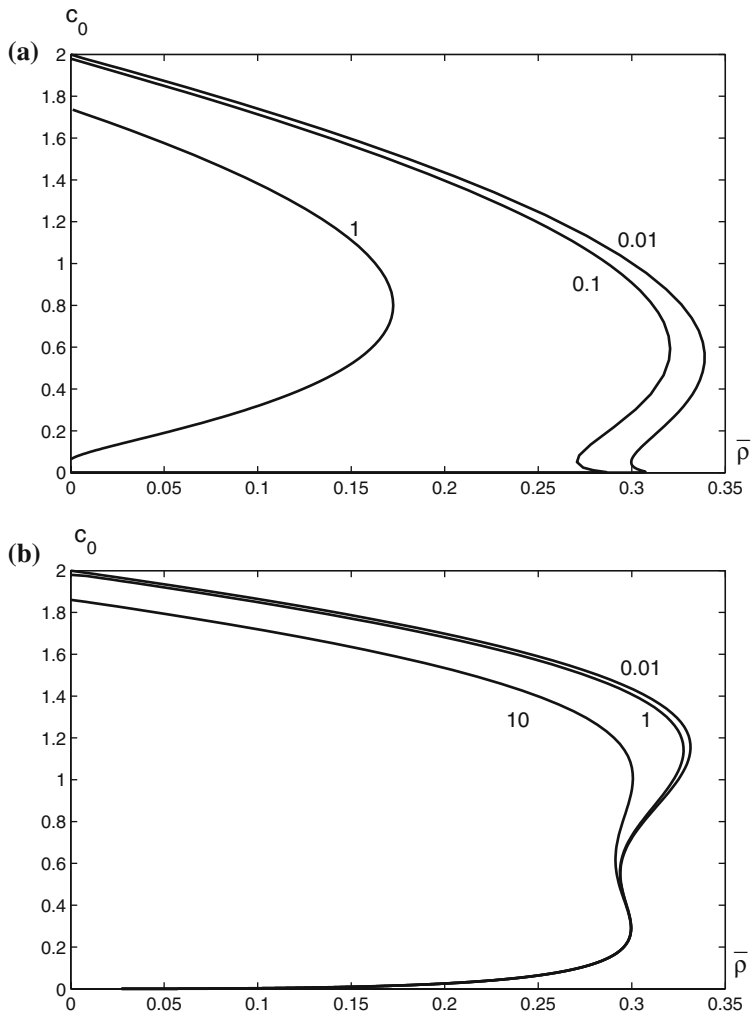

Figure 10. $c_0 - \overline{\rho}$ curves for a range of values of $\overline{\alpha} > 0$ obtained from the numerical integration of equations (75,76) for (a) $\overline{\beta} = 0.1$, $\mu = 0.15$, (b) $\overline{\beta} = 100.0$, $\mu = 5.5$, $L_A = L_W = 1$.

Using equation (73) to eliminate S_1 from equation (72) gives

$$\overline{\beta}U_0 + \overline{\alpha}w_0 = \frac{\overline{\alpha}^2 c_0 + \overline{\rho}\overline{\beta}^2 I_1 T_1}{\overline{\alpha}c_0 - \overline{\rho}\overline{\beta}I_1} \equiv R_0(c_0, T_1) \tag{74}$$

Equation (74) can then be used to eliminate w_0 from equation (59) to give

$$U_0'' - c_0 U_0' + (R_0 - \overline{\beta}U_0)\,\mathrm{e}^{-\mu U_0} = 0 \tag{75}$$

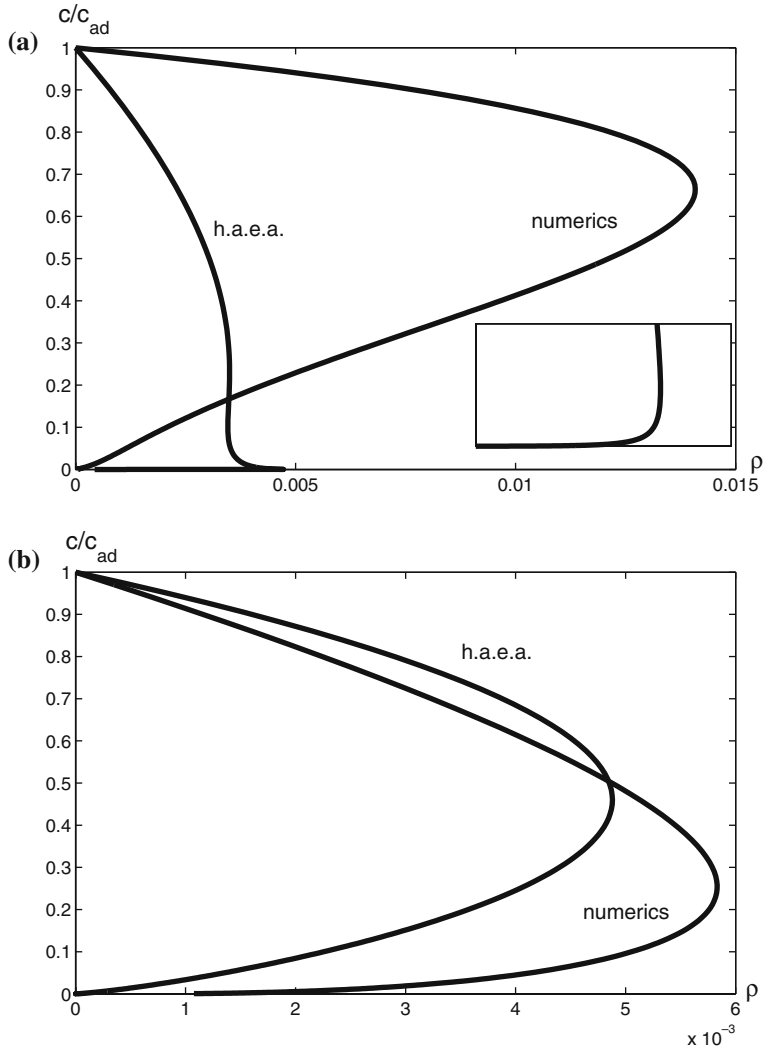

Figure 11. Comparison of the wave speeds for the high activation energy analysis and those obtained numerically with $\varepsilon = 0.1$ and $\alpha = 0$, plots of c/c_{ad} for (a) $\beta = 10^{-4}$, $\mu = 0.1$, (b) $\beta = 10^{-2}$, $\mu = 1.5$, $L_A = L_W = 1$.

subject to the boundary conditions

$$U_0 \sim -T_1 - \frac{c_0\overline{\alpha}(c_0T_1 + \overline{\rho}I_1)}{\overline{\alpha}c_0 - \overline{\rho}\overline{\beta}I_1}\,Y + \cdots \quad \text{as } Y \to 0, \quad U_0' \to 0 \quad \text{as } Y \to \infty \tag{76}$$

(the latter condition implies that $U_0 \to R_0/\overline{\beta}$ as $Y \to \infty$), with c_0 related to T_1 by equation (49).

This system reduces to the one discussed in [12] when $\overline{\rho} = 0$ and $L_A = 1$, where it was seen that up to three solutions were possible. We can integrate equations (75,76) numerically, following [12]. The singularity in R_0 when $\overline{\alpha} c_0 = \overline{\rho}\overline{\beta} I_1$ is removable, since equation (73) gives $T_1 = -\overline{\alpha}/\overline{\beta}$ in this case. We solved equations (75,76) with $\overline{\alpha} > 0$ for the two cases shown in figure 9 (when $\overline{\alpha} = 0$). The results are shown in figure 10. The existence of four solution branches continues to relatively large values of $\overline{\alpha}$ for $\overline{\beta} = 100$ (figure 10(b), even with $\overline{\alpha} = 10.0$ the curve has a similar form to that shown in figure 9(b). However these additional solution branches disappear at much smaller values of $\overline{\alpha}$ for $\overline{\beta} = 0.1$.

5. Conclusions

We have considered the conditions for flame propagation and flame inhibition in a model driven by an exothermic reaction subject to inhibitory chemical processes. These consisted of the endothermic decomposition of an inhibitor species W leading to the formation of a 'radical scavenger' S, which could then act as a catalyst for the removal of active radical X through an additional termination step. The first process is characterised by the parameter α and the second by the parameter ρ. These parameters, which, respectively, measure the rate of heat loss through the endothermic reaction relative to the rate of heat generation by the combustion reaction and the fraction of radical scavenger molecules produced by the decomposition of W, together with the parameter β, which measures the rate at which W is consumed relative to the fuel, are the important ones in determining the conditions for flame inhibition. Each process on its own can fully inhibit flame propagation. The effect of only the first process (i.e. when $\rho = 0$) was investigated fully in [7,12,13]. It was found that there is flame quenching in certain domains of the (μ, β) parameter plane, i.e. the (α, c) curve has a turning point, for appropriate values of μ and β. In fact, the curve is folded into a characteristic S-shape, showing bi-stability between upper and lower branches of steady solutions separated by a branch of saddle point solutions. Otherwise flames were possible for all α, though had considerable reductions in speed as α increased.

A new feature caused by the addition of the radical scavenger is that the (α, c) curve has a turning point for any (μ, β) parameter pair provided ρ is sufficiently large, (for $\mu \leqslant 1$, it has a turning point for any positive ρ). Thus, for any $\rho \neq 0$, there is a critical value of α for flame propagation. Above this critical value the flame cannot be established, i.e. the system has only the trivial solution. An additional feature of our model is that for small positive values of ρ there can be four solutions below the critical value of α. That is the (α, c) curve can have three turning points for suitable values of μ and β. Bounds on the parameter μ for the possible existence of four solution branches were provided by the high activation enegy asymptotics, equation (71).

For different values of the parameters L_A, L_W, β and μ, the dependence of the flame speed c as a function of α and ρ were determined numerically. As in the scavenger-free ($\rho = 0$) case it was found that the (μ, β) parameter plane can be divided into three regions according to the shape of the (α, c) curve [12, 13]. A given horizontal line (β fixed) in the (μ, β) parameter plane intersects all three regions. For a given value of β we can have the following three cases. For small values of μ the (α, c) curve can have three or one turning point depending on the value of ρ, that is the system can have four, two or zero solutions. The evolution of the (α, c) curve as ρ is varied is shown in figure 2. For larger values of μ the (α, c) curve has one turning point if $\rho > 0$, so that the system has two solutions if α is below its critical value. The evolution of the (α, c) curve as ρ is varied is shown in figure 3. Increasing the value of μ further the (α, c) curve may be monotone even for positive values of ρ, i.e. there is no quenching value of α. However, for larger positive values of ρ the (α, c) curve has a turning point, i.e. α has a critical value, above which there is no flame propagation. The evolution of the (α, c) curve in this case is shown in figure 4. The high activation energy asymptotics also revealed that, for even higher values of μ, the situation in which there are four solution branches returns.

We can compare the values of the wave speed c from the high activation energy analysis with those obtained numerically with $\varepsilon = 0.1$. We concentrate on the $\alpha = 0$ case and take $L_A = L_W = 1$. To make this comparison we plot c/c_{ad} against ρ for two cases, for a small value of μ ($\mu = 0.1$, $\beta = 10^{-4}$) shown in figure 11(a), and for a larger value of μ ($\mu = 1.5$, $\beta = 10^{-2}$) shown in figure 11b. In the latter case there is reasonable agreement between the two sets of results. Both curves have the same shape and have critical values for ρ differing by about 15%, the value determined by the numerical integrations being slightly higher. In the former case (figure 11(a)) the curves have a similar form (both having four solution branches – as shown in the inset for the numerical solutions) though the values for the two cases are very different. This suggests that very little quantitative information is provided by the high activation energy asymptotics for this value of ε and a much smaller value of ε would be required for better agreement. The need for very small values of the activation energy parameter to get reasonable agreement with results from the high activation energy analysis has been discussed in Ref. 18 and reasons for it have been advanced. These appear to apply, at least in certain parameter ranges, in our model as well.

Acknowledgments

This work was supported by the EPSRC (Grant GR/N66537/01). The authors also wish to acknowledge the support received from the ESF Programme REACTOR and the OTKA grant F034840.

References

[1] J.D. Buckmaster, The quenching of deflagration waves, Combustion and Flame 26 (1976) 151–162.

[2] V. Giovangigli, Nonadiabatic plane laminar flames and their singular limits, SIAM J. Math. Anal. 21 (1990) 1305–1325.

[3] W.J.F. Govaerts, *Numerical methods for bifurcations of dynamical equilibria*, SIAM, (Philadelphia, PA, 2000).

[4] B.F. Gray, S. Kalliadasis, A. Lazarovici, C. Macaskill, J.H. Merkin and S.K. Scott, The suppression of an exothermic branched–chain flame through endothermic reaction and radical scavenging, Proc. R. Soc. Lond. A, 458 (2002) 2119–2138.

[5] G. Joulin, A. Liñan, G.S.S. Ludford, N. Peters and C. Schmidt-Laine, Flames with chain-branching/chain-breaking kinetics, SIAM J. Appl. Math., 45 (1985) 420–434.

[6] D.G. Lasseigne, T.L. Jackson and L. Jameson, Stability of freely propagating flames revisited, Combust. Theory Modelling, 3 (1999) 591–611.

[7] A. Lazarovici, S. Kalliadasis, J.H. Merkin and S.K. Scott, Flame quenching through endothermmic reaction, J. Eng. Math. 44 (2002) 207–228.

[8] A. Lazarovici, S. Kalliadasis, J.H. Merkin, S.K. Scott and P.L. Simon, The propagation and inhibition of an exothermic branched-chain flame with an endothermic reaction and radical scavenging. J. Eng. Math. 49 (2004) 41–55.

[9] M. Marion, Qualitative properties of a nonlinear system for laminar flames without ignition temperature, Nonlinear Anal. 9 (1985) 1269–1292.

[10] P.L. Simon, S. Kalliadasis, J.H. Merkin and S.K. Scott, Quenching of flame propagation with heat loss, J. Math. Chem. 31 (2002) 313–332.

[11] P.L. Simon, S. Kalliadasis, J.H. Merkin and S.K. Scott, Quenching of flame propagation through endothermic reaction, J. Math. Chem. 32 (2002) 73–98.

[12] P.L. Simon, S. Kalliadasis, J.H. Merkin and S.K. Scott, Inhibition of flame propagation by an endothermic reaction, IMA J. Appl. Math. 68 (2003) 537–562.

[13] P.L. Simon, S. Kalliadasis, J.H. Merkin and S.K. Scott, Stability of flames in an exothermic-endothermic system, IMA J. Appl. Math. 69 (2004) 175–203.

[14] J. Warnatz, U. Maas and R.W. Dibble, *Combustion. Physical and Chemical Fundamentals, Modeling and Simulation, Experiments, Pollutant Formation* (Springer, Berlin 2001).

[15] A.I. Volpert, V.A. Volpert and V.A. Volpert, *Traveling Wave Solutions of Parabolic Systems*, (AMS, Providence, RI,1994). (Translated from Russian Manuscript by J.F. Heyda. Translations of Mathematical Monographs, 140.)

[16] R.O. Weber, G.N. Mercer, H.S. Sidhu and B.F. Gray, Combustion waves for gases ($Le = 1$) and solids ($Le \to \infty$), Proc. Roy. Soc. Lond. A, 453 (1997) 1105–1118.

[17] Ya.B. Zeldovich, G.I. Barenblatt, V.B. Librovich and G.M. Makhviladze, *The Mathematical Theory of Combustion and Explosions* (Consultants Bureau, 1985).

[18] J.W. Dold, R.W. Thatcher and A.A. Shah, High order effects in one step reaction sheet jump conditions for premixed flames, *Combust. Theory Modelling* 7 (2003) 109–127.